

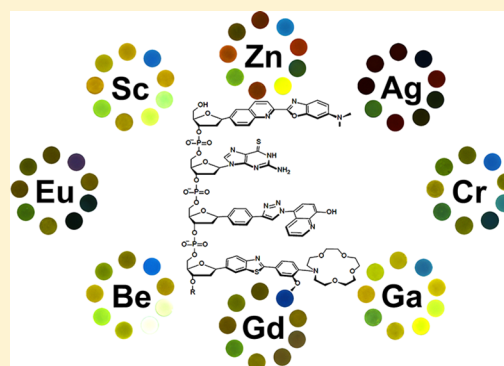
# Large-Scale Detection of Metals with a Small Set of Fluorescent DNA-Like Chemosensors

Lik Hang Yuen, Raphael M. Franzini,<sup>†</sup> Samuel S. Tan, and Eric T. Kool\*

Department of Chemistry, Stanford University, Stanford, California 94305, United States

## S Supporting Information

**ABSTRACT:** An important advantage of pattern-based chemosensor sets is their potential to detect and differentiate a large number of analytes with only few sensors. Here we test this principle at a conceptual limit by analyzing a large set of metal ion analytes covering essentially the entire periodic table, employing fluorescent DNA-like chemosensors on solid support. A tetrameric “oligodeoxyfluoroside” (ODF) library of 6561 members containing metal-binding monomers was screened for strong responders to 57 metal ions in solution. Our results show that a set of 9 chemosensors could successfully discriminate the 57 species, including alkali, alkaline earth, post-transition, transition, and lanthanide metals. As few as 6 ODF chemosensors could detect and differentiate 50 metals at 100  $\mu$ M; sensitivity for some metals was achieved at midnanomolar ranges. A blind test with 50 metals further confirmed the discriminating power of the ODFs.



## INTRODUCTION

Colorimetric and fluorescent chemosensors have served as detection tools for many chemical species<sup>1–3</sup> as they can provide sensitive real-time responses, easily interpreted outputs, access to biological systems, and structural tunability to fit the application. While the conventional sensing approach has used one sensor per analyte, much recent attention has been focused on developing differential or array sensors, in which a pattern of responses from promiscuous sensor compounds enables analyte discrimination. In addition to being less labor intensive to develop than analyte-specific sensors, differential sensors can discriminate a larger number of analytes than actual elements in the array by analysis of the combined pattern of responses.<sup>4</sup> This feature lowers the cost and burden of synthesizing large numbers of sensor molecules and simplifies analysis. Prominent examples have been reported for differentiating 19 toxic industrial chemicals with 36 chemically responsive pigments,<sup>5</sup> 5 serum proteins with fluorescent protein–nanoparticle conjugates,<sup>6</sup> 5 metals with 1 dye and 5 thiols,<sup>7</sup> and 10 volatile organic compounds with 4 fluorescent oligomers.<sup>8</sup>

We have recently explored the use of DNA mimics with fluorescent nucleobase surrogates<sup>9</sup> as pattern-based sensors. These oligodeoxyfluorosides (ODFs) exhibit complex electronic and structural interactions between the proximal fluorophores, which can provide widely varied fluorescence responses when interacting with analytes. Assembling fluorophores on a DNA backbone enables rapid automated synthesis of such chemosensors on solid supports via a DNA synthesizer, and the water-soluble free molecules can be released and used in dissolved form if desired.<sup>10</sup> From previous combinatorial libraries of ODFs, we have identified sensor compounds that respond to metal ions,<sup>10</sup> organic volatiles,<sup>11</sup>

toxic gases,<sup>12</sup> bacterial metabolites,<sup>13</sup> and food spoilage.<sup>14</sup> As mentioned above, pattern-based sensing offers the intriguing potential for discriminating many more analytes than sensor compounds. However, to date this possibility has been tested with only moderate numbers of analytes. Here we test this principle at a conceptual limit, by attempting to detect and discriminate nearly all water-soluble metals and metalloids in solution. We have recently described a library of 6,561 ODF tetramers on polyethylene glycol (PEG)–polystyrene beads that showed high sensitivity toward eight heavy metals.<sup>15</sup> Using the same library, we identified a small set of sequences that are effective in yielding strong and varied fluorescence responses to a broad range of metal ions. We report that a set of as few as 6 tetramers on beads can be used to discriminate 50 different metal species at micromolar concentrations in aqueous buffer, and 48 out of 50 metal ions were correctly identified in a blind test, confirming the discrimination power of the ODF molecular design.

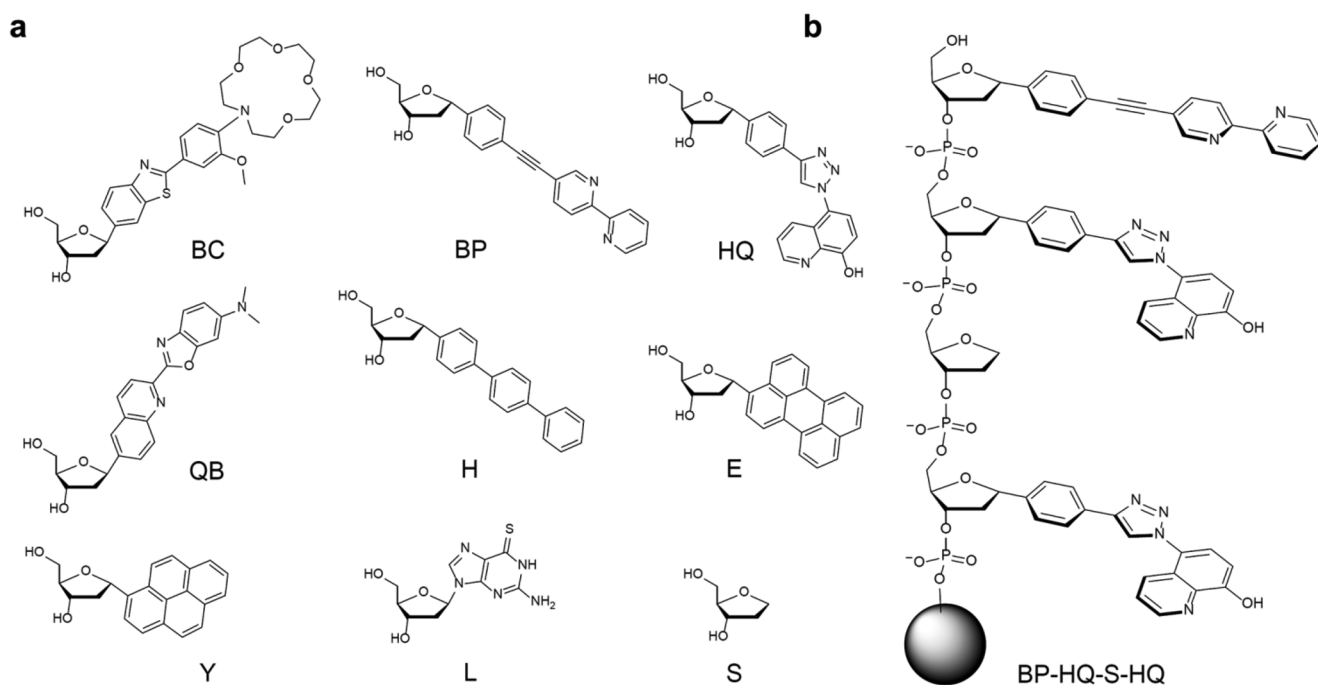
## EXPERIMENTAL SECTION

**ODF Synthesis.** ODFs were assembled on an Applied Biosystems DNA synthesizer via standard phosphoramidite chemistry on a 1  $\mu$ mole scale with one sequence per bead. Extended coupling times (15 min) were used to maximize coupling yields. Monomers and the tetramer library were prepared as described.<sup>9,15</sup> ODFs were characterized by MALDI-MS and absorption/emission spectra by concurrently preparing samples for analysis using controlled-pore glass (CPG) support.

**Imaging and Analysis of Metal Ion Responses.** Imaging was done in a small Petri dish (Tissue Culture Dish 35  $\times$  10 mm, Falcon)

Received: August 3, 2014

Published: September 25, 2014



**Figure 1.** ODFs described in this study. (a) Monomers included in the metal ion sensing library. (b) Representative structure of an ODF: BP-HQ-S-HQ (sequence named 5' → 3'). The sphere represents a PEG-polystyrene bead, 130 μm diameter.

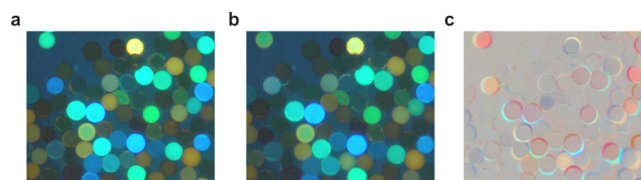
secured on a microscope slide with double-sided tape. A double-sided tape was adhered inside the dish and ODF beads (~5 beads) were spread out on the tape and gently pressed down. The beads were submerged and incubated in 2 mL buffer (5 mM 2,4,6-collidine- $\text{HNO}_3$ , pH 7.3) for 10 min, then imaged using a 4× objective of an epifluorescence microscope with the exposure setting adjusted so that the beads were properly exposed (before image;  $\lambda_{\text{ex}} = 325\text{--}375\text{ nm}$ ;  $\lambda_{\text{em}} > 420\text{ nm}$ ). The buffer was then exchanged with the metal ion solution with the targeted concentration in the same buffer. The Petri dish was covered and incubated in the dark for 24 h. Second image was then taken with the same exposure setting (after image). The before/after images were digitally superimposed using Adobe Photoshop with the inverse-colored "before" image at the bottom and the "after" image overlaid with 50% transparency to give the grayscale difference image (see Figure 2c).

Data were obtained by recording  $\Delta$  RGB values of individual beads in Adobe Photoshop. A  $32 \times 32$  pixel box was used to capture pixels at the center of each bead, and the average  $\Delta$ RGB values within the box were recorded in an Excel file. The experiment was repeated twice, and 6 sets of  $\Delta$ RGB values were recorded per metal per sequence. Control values were also obtained in the same fashion by incubating the beads in buffer for 24 h. The control  $\Delta$ RGB values were then averaged and subtracted from the corresponding values of each metal. The resulting gray-scale RGB changes were then multiplied by 2 to obtain the full RGB changes. These  $\Delta$ RGB values were processed using statistical analysis program XLSTAT (Addinsoft Inc.) and analyzed by discriminant analysis and agglomerative hierarchical clustering (See Experimental Methods in Supporting Information).

## RESULTS AND DISCUSSION

**Library Construction, Screening, and Decoding.** To find metal-responsive ODF sequences, we employed a combinatorial library composed of tetramer-length sequences with 9 distinct monomers on 130 μm polystyrene beads as described.<sup>9</sup> As monomers, the library included simple fluorescent nucleosides (Y and E)<sup>9</sup> and spacers (H, L, S)<sup>10</sup> to diversify the fluorophore interactions, and four fluorescent ligands<sup>15</sup> (BC, BP, HQ, and QB) for metal binding (Figure 1). These latter four—inspired by known fluorescent metal

ligands<sup>16–19</sup>—were expected to exhibit diverse affinities to a range of metals. All nucleosides were appended with 5'-dimethoxytrityl and 3'-phosphoramidite groups to allow their use in library construction with standard split-and-mix procedure employing a DNA synthesis cycle.<sup>9</sup> The resulting ODF library shows a large variation in emission colors and intensity under the epifluorescence microscope (excitation filter 340–380 nm; long-pass emission  $>420\text{ nm}$ ; Figure 2).



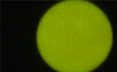
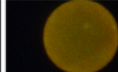






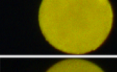
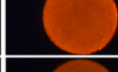
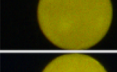
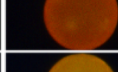
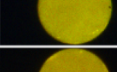
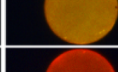
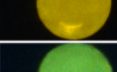

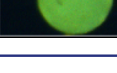

**Figure 2.** Sample images of ODF library under an epifluorescence microscope ( $\lambda_{\text{ex}} = 340\text{--}380\text{ nm}$ ;  $\lambda_{\text{em}} > 420\text{ nm}$ ) (a) before and (b) after exposure to Zn(II) and (c) their inverse overlay, in which beads that show nongray colors contain ODFs responding to Zn(II). The before/after images were digitally superimposed with the inverse-colored "before" image at the bottom and the "after" image overlaid with 50% transparency to give difference image (c). 50% gray color indicates no change from (a) to (b); beads lighter than 50% gray indicate lighting up responses to the metal, while darker beads indicate quenching responses. Colors indicate color shifts.

As analytes, we included essentially all the water-soluble metal ions (57 species in total) to broadly test the differentiation power of these ODFs. For metals with multiple redox states, we chose the most common or stable form. Where water-soluble sodium or nitrate salts were unavailable, the ammonium, oxide, chloride, or fluoride salts were used (Supporting Information, Table S1).

To prevent fluorescence changes due to pH, we used 5 mM 2,4,6-collidine- $\text{HNO}_3$  (pH 7.3) as this buffer was shown to be a weak metal ligand.<sup>20</sup> We performed screening experiments by

incubating the beads in 250 and 1  $\mu\text{M}$  buffered metal ion solutions for 1 h and successfully identified and decoded<sup>21</sup> 174 ODF sequences that responded strongly to a test set of 36 metal ions (see Figure 2 for an example). From these 174 candidates we selected 9 sequences for resynthesis aiming to diversify monomers in the sequences, color of the ODFs, the metal to which the sequence responded, the type (quenching, lighting up or color change) and amplitude of fluorescence changes in the sensor set (Table 1). The chosen sequences

**Table 1. Images of Selected ODF Sequences on Beads before and after Exposure to Cd(II) at 100  $\mu\text{M}$**

Sequence	Before	Cd(II)
5'-BC-QB-H-H-3'		
5'-BP-H-S-S-3'		
5'-BP-HQ-S-HQ-3'		
5'-S-HQ-HQ-HQ-3'		
5'-QB-E-Y-Y-3'		
5'-QB-H-E-S-3'		
5'-QB-L-HQ-BC-3'		
5'-QB-L-H-QB-3'		
5'-Y-HQ-BC-E-3'		

were simultaneously synthesized both on 130  $\mu\text{m}$  polystyrene beads for sensing and on CPG for characterization. The ODFs on the CPG were cleaved and deprotected, purified by HPLC, and characterized by mass spectrometry (Supporting Information, Table S2), absorption and emission spectra (Supporting Information, Figure S1).

We cross-screened the full set of 57 metals with our 9 sensors on beads, using 100  $\mu\text{M}$  to evaluate the detection and differentiation of this broad range of metal species (See Table 1 for an example). At this concentration, 50 of 57 metals were discriminated (see analyses below); the remaining 7 (alkali metals, Re and W), however, required higher concentrations for successful discrimination. Taken as a whole, the sensor compounds showed highly varied emission changes but retained reproducible responses for each metal tested (see  $\Delta\text{RGB}$  data in Supporting Information, Figure S2).

**Detection and Differentiation of Alkali Metals.** Due to their low charge density,<sup>22</sup> alkali metal ions are notoriously difficult to detect and differentiate via fluorescence chemosensors and require relatively high metal concentrations.<sup>17,23</sup> During the experiments, we found that incubating the beads for 24 h provided enough time for most of the metals to reach equilibrium and yielded stronger and more reproducible results, and hence this procedure was used for the remaining study. We

measured the responses of the 9-ODF set with the five alkali metals ( $\text{Li}^+$ ,  $\text{Na}^+$ ,  $\text{K}^+$ ,  $\text{Rb}^+$ ,  $\text{Cs}^+$ ) at 100 mM. Of the identified responding ODFs, sequences containing BC showed relatively strong responses, suggesting that the crown ether substructure of BC may assist in recognition of the alkali metals. Significantly, the relatively small responses to alkali metals at lower concentrations were beneficial to the rest of our studies as we used a number of anionic metal complexes as analytes with sodium or potassium counterions. Background signals from these counterions were thus minimized in subsequent experiments.

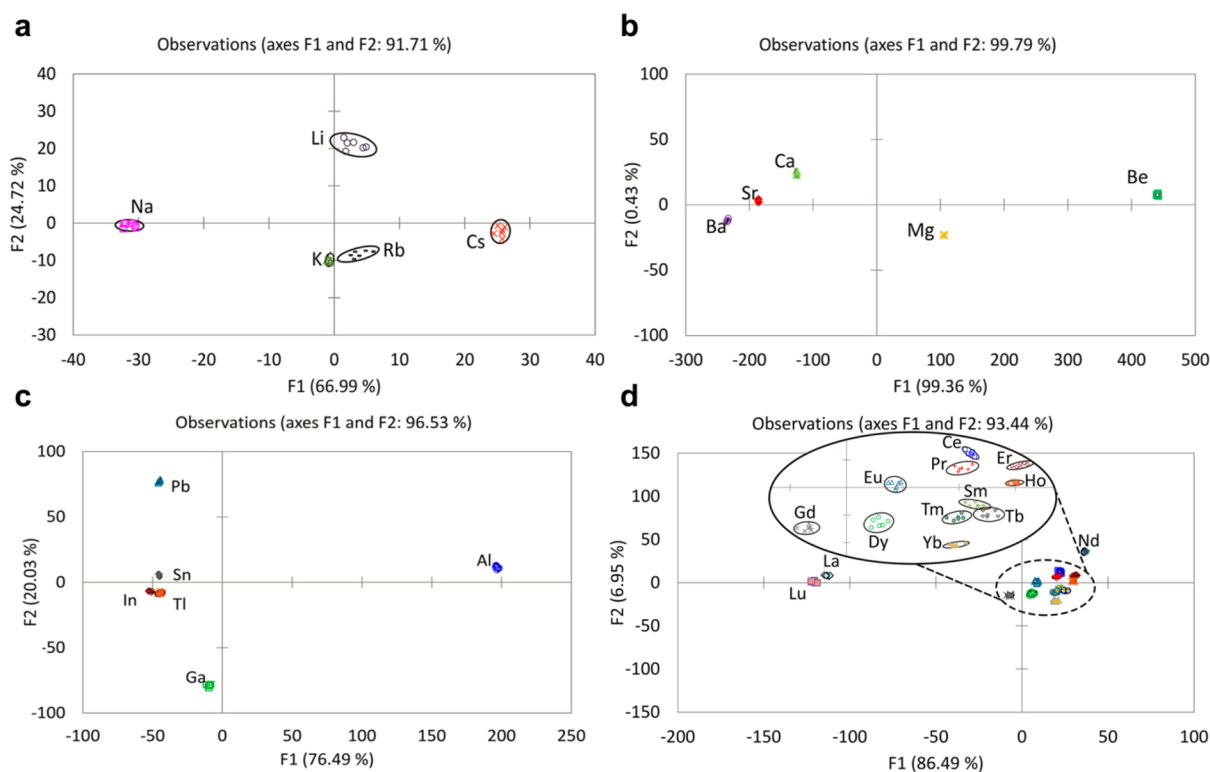
Each sensing response for a given metal was measured with six separate beads to test reproducibility, and changes in fluorescence intensity were quantified in red, green, and blue color channels, generating  $\Delta\text{RGB}$  data (Supporting Information, Figure S2). To quantitatively evaluate responses of the nine chemosensors as a pattern, we employed discriminant analysis (DA) and agglomerative hierarchical clustering (AHC). The analyses confirm successful differentiation of all five metals at 100 mM. Based on the DA, pattern responses from  $\text{Li}^+$ ,  $\text{Na}^+$ , and  $\text{Cs}^+$  are strongly differentiated (Figure 3a), while responses to  $\text{K}^+$  and  $\text{Rb}^+$  are clustered more closely. The 95% confidence circles for the five metals are well separated even in the first two dimensions with 91.7% of the discrimination captured. “Leave-one-out” analysis—a technique performed with DA to evaluate the validity of the analysis of the data set—reveals 80% identification accuracy for the alkali metals, with  $\text{K}^+$  and  $\text{Rb}^+$  most likely to be confused. The AHC analysis shows similar results (Supporting Information, Figure S3), with all of the experimental trials from each metal clustered and distinct from the other metals.

**Detection and Identification of Other Metals at 100  $\mu\text{M}$ .** Alkaline earth metals revealed much stronger responses than alkali metals, even at  $10^3$ -fold lower concentration. Notably, ODF sequences containing multiple HQ monomers (e.g., S-HQ-HQ-HQ and BP-HQ-S-HQ) showed a strong lighting-up response, whereas sequences with a single HQ did not (Y-HQ-BC-E and QB-L-HQ-BC), implying cooperative metal binding by multiple monomers. This lighting-up response was period-dependent, with  $\text{Be}^{2+}$  being the strongest, while other sequences showed similar quenching independent of period (Supporting Information, Figure S2).

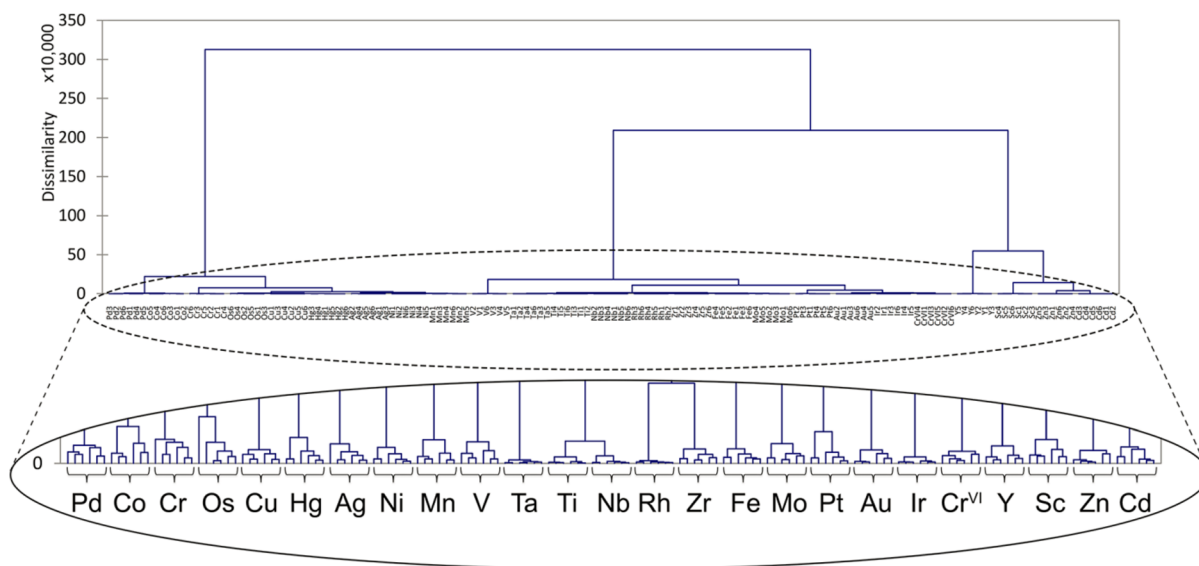
The DA plot shows distinct separation outside the 95% confidence circles with F1 capturing 99.36% of the discrimination (Figure 3b); the high discrimination captured on F1 indicates that the use of an array and multivariate statistical analysis tools might be unnecessary<sup>4</sup> as the differential responses from the five metals predominantly come from S-HQ-HQ-HQ and BP-HQ-S-HQ (see quantitative responses of ODF sensors in Supporting Information, Figure S2). Because of the sufficient differential responses from S-HQ-HQ-HQ and BP-HQ-S-HQ, “leave-one-out” analysis shows differentiation with 100% identification accuracy;  $\text{Ca}^{2+}$ ,  $\text{Sr}^{2+}$ ,  $\text{Ba}^{2+}$  and  $\text{Be}^{2+}$ ,  $\text{Mg}^{2+}$  form two distinct subgroups in the AHC dendrogram (Supporting Information, Figure S4).

Next we turned to the analysis of six post-transition metals at 100  $\mu\text{M}$ : Al(III) and Ga(III) illuminated the multi-HQ sequences; Pb(II) quenched all the sequences, while In(III), Sn(II), and Tl(I) yielded weaker but characteristic signals (Supporting Information, Figure S2). DA and AHC reveal complete differentiation of all six post-transition metals (Figure 3c and Supporting Information, Figure S5) with 100% identification accuracy according to “leave-one-out” analysis.





**Figure 3.** Discriminant analysis plots of ODF responses to (a) alkali metals, (b) alkaline earth metals, (c) post-transition metals, and (d) lanthanides. 95% confidence circles are shown in each figure. Note that some of the circles are covered by the data points. Metal concentrations are 100 mM in (a) and 100  $\mu$ M in (b–d). Data were obtained by imaging beads containing ODFs after 24 h incubation in metal solutions (See Experimental Methods in Supporting Information for interpretation of the DA plots).

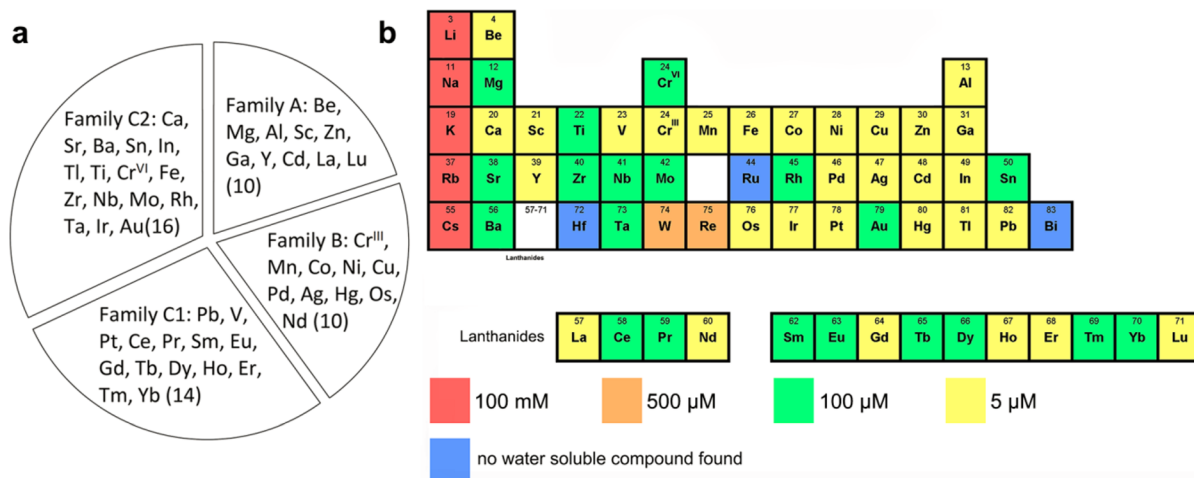


**Figure 4.** Dendrogram from agglomerative hierarchical clustering (AHC) of detecting 25 transition-metal ions at 100  $\mu$ M with nine ODF sensors in buffered deionized water grouped by similarities of response. Note that all the experimental trials of each metal are grouped together.

As expected, the three metals yielding smaller  $\Delta$ RGB signals (In(III), Tl(I), and Sn(II)) lie closest on the DA and AHC plots, while those that show strong signals (Al(III), Ga(III), and Pb(II)) are more widely separated.

For the lanthanide series, we tested the 14 nonradioactive metals at 100  $\mu$ M. Notable among the responses from the nine sensors were strong lighting up by La(III) and Lu(III) (e.g., with S-HQ-HQ-HQ and BP-HQ-S-HQ), strong quenching by Nd(III) (all sequences), and color shifts with Eu(III) (a distinct

blue shift with BP-H-S-S) and Gd(III) (with red shifts of S-HQ-HQ-HQ and BP-HQ-S-HQ). The remaining nine lanthanides, which yielded smaller color shifts and quenching patterns, were grouped more closely (Figure 3d). Lanthanides are known to be difficult to differentiate because of their similar chemical properties; for example, almost no differentiation was found between Eu(III) and Gd(III) even at 10 mM in a previous report.<sup>24</sup> However, the discrimination in the current study using ODFs between the 14 lanthanides is clear even in



**Figure 5.** Summary of (a) AHC analysis of the cross screening between 9 chemosensors and 50 metals at 100 μM. Four major classes of response were observed in our AHC data. The numbers in the parentheses indicate the number of metals in that subfamily and (b) discrimination power of nine ODF sequences at various metal concentrations for 57 metal species. Colors denote the lowest concentrations for which a species was successfully detected and differentiated.

the 2-D DA plot. “Leave-one-out” analysis validates the high cross-responsiveness of ODFs toward lanthanides, showing 100% identification accuracy. AHC also clearly groups each experimental trial together, demonstrating high repeatability that enables discrimination even with small differences in response (Supporting Information, Figure S6).

For the transition metals, we excluded Hf and Ru due to their low aqueous solubility but included Cr(VI) along with Cr(III), as both are important stable oxidation states of Cr. Among the 27 metals tested, our sensors displayed a broad variety of response signals for 25 species at 100 μM. The sensors failed to show responses over background at 100 μM to the oxoanions of Re(VII) and W(VI), but detectable responses were seen at 500 μM (Supporting Information, Figure S7). Notable trends included strong fluorescence responses with the first-row transition metals except for Fe(III) and Ti(IV). Metal anionic complexes usually showed medium to weak signals (Ti(IV), Cr(VI), Zr(IV), Nb(V), Mo(VI), Rh(III), Ta(V), W(VI), Re(VII), Ir(IV), and Pt(II), except Os(VI)), possibly due to the dearth of accessible ligand binding sites on the metals. In general, we found that chloride complexes (Rh(III), Ir(IV) and Pt(II)) yielded stronger responses than oxide (Cr(VI) and Mo(VI)) and fluoride complexes (Ti(VI), Zr(IV), Nb(V) and Ta(V)), probably due to the strong metal-oxygen and -fluoride bonds. S-HQ-HQ-HQ and BP-HQ-S-HQ became brighter when exposed to Group III metals (Y(III) and Sc(III)). Cd(II) and Zn(II) color-shifted the QB containing sequences and illuminated only S-HQ-HQ-HQ. However, these trends shared by Cd(II) and Zn(II) were absent in the last d<sup>10</sup> metal, Hg(II), which yielded quenching with all sequences, thus allowing ready differentiation from the former metals.

The 25 transition metals all showed significant signals above background at 100 μM. DA separates the metals that provided strong lighting up responses and clusters those that gave strong quenching and weak signals into two groups (Supporting Information, Figure S8). “Leave-one-out” analysis confirms this finding, showing that the accuracy of the differentiation is 99.33%. Complete differentiation of all 25 transition metals is also observed with AHC analysis (Figure 4).

As a control experiment, we also measured the fluorescence responses of the ammonium, chloride and fluoride counterions

in the same buffer content. Only minimal signals were observed at 100 μM, confirming that the fluorescence changes of ODFs indeed came from the metals (Supporting Information, Figure S9).

**Analysis of the Entire Set of Metal Ions.** To explore the number of metals this chemosensor set can differentiate, we used the ΔRGB values obtained with all sensors and 50 metals at 100 μM and performed an overall AHC analysis. AHC successfully grouped all the trials from each metal in a subgroup, showing complete differentiation of 50 metals. On the dendrogram, three chief families of response are seen (Figure 5 and Supporting Information, Figure S10): Family A contains metals that yielded turn-on signals with at least one of two sequences (S-HQ-HQ-HQ and BP-HQ-S-HQ) and family B metals strongly quenched most sequences. Family C can be divided into two subfamilies C1 and C2: C1 includes many lanthanides and other metals that provided moderate changes, and C2 contains metals that only yielded moderate to small changes. DA with “leave-one-out” analysis shows that identification accuracy is 99.67%. Thus, we conclude that the 9 sensors as a set can show diverse responses of sufficient magnitude to identify 50 different metals at 100 μM.

As a more restrictive test of the signal diversity in these DNA polyfluorophore compounds, we sought to determine the minimal number of sequences required to differentiate the 50 metals detected at 100 μM. We found that only 6 of the 9 sequences (BP-H-S-S, BP-HQ-S-HQ, S-HQ-HQ-HQ, QB-H-E-S, QB-L-H-QB and QB-L-HQ-BC) are sufficient to differentiate 48 of these 50 metals, with only a slight mixing between Cu(II) and Ni(II) (Supporting Information, Figure S11). These last two metals strongly quenched all sequences, but they can be easily differentiated at a lower concentration where differential quenching is seen (see below).

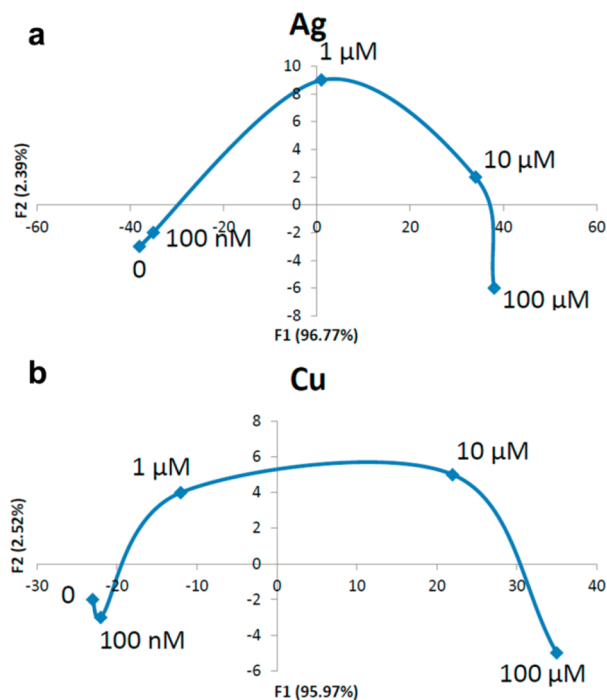
The broad data set also allowed us to evaluate the individual ODFs to measure their diversifying power. From the AHC analysis of the individual sequences toward the 50 analyzed metals, we observed that the sequence S-HQ-HQ-HQ alone, which shows the most diverse signals, can differentiate 15 metals due to its ability to exhibit strong quenching (e.g., Ni(II) and Cu(II)), lighting up (Be(II) and Al(III)), and color change (Ga(III) and Gd(III)) responses toward the analytes

(Supporting Information, Figure S12). Thus, 130  $\mu\text{m}$  beads each containing  $\sim 1$  pmole of a single ODF dye can be used to distinguish up to 15 different analytes from 57 possibilities in a few drops of solution by simple fluorescence imaging.

To test the sensitivity of the ODF chemosensors, we evaluated responses of the 9-ODF set with 50 metals at 20-fold lower concentration (5  $\mu\text{M}$ ). As expected, the overall amplitude of fluorescence changes decreased. However, the AHC analysis revealed that 30 of 50 metals can still be differentiated (Supporting Information, Figure S13). For those that showed overlapping signals, many were metal anionic complexes (Cr(VI), Ti(IV), Zr(IV), Nb(V), Mo(VI), and Rh(III)). Figure 5 summarizes our screening results. Overall, these sensors are most sensitive toward transition metals and least sensitive to the alkali metals, with lanthanides, alkaline earths, and post-transition metals falling in the intermediate range.

As a sensitivity comparison between the current and previous sets of ODF metal sensors,<sup>10</sup> we titrated BP-H-S-S in solution with varying concentrations of Co(II), Cu(II), and Ni(II) from 1 nM to 100  $\mu\text{M}$ . Similar to the earlier study, the titration curves appeared to be sigmoidal, consistent with one-site binding at the tested concentration range (Supporting Information, Figure S14). The new ODF showed high binding affinity toward Cu(II), Ni(II), and Co(II), with binding transitions at midnanomolar ranges. The enhanced sensitivity may reflect stronger metal ligands in the current library.

We further examined the concentration dependence of the 6-ODF set toward 8 selected metals representing alkaline earth, post-transition, transition metals and lanthanides to approximate the detection limit and the dynamic range of the ODF sensors (Figure 6 and Supporting Information Figures S15 and S16). The 6 ODFs exhibited strong responses between 100 and 1  $\mu\text{M}$ , but the signals decreased below 1  $\mu\text{M}$  except with Ag(I) and Cu(II), which remained relatively strong above 100 nM



**Figure 6.** Concentration curves plotted using the centroids of six replicates from the discriminant analysis for (a) Ag(I) and (b) Cu(II). Concentrations are noted next to the centroids.

(Figure 6). This indicates that the detection limits of these ODFs on solid supports for most of the metals are in the low micromolar to high nanomolar range.

Finally, as a rigorous test of the differentiation power of ODFs, we prepared 50 unknown metal ion solutions—each containing 100  $\mu\text{M}$  of one metal—as a blind experiment using the minimal 6-ODF set described above. Using the  $\Delta\text{RGB}$  values from both the unknown and 100  $\mu\text{M}$  reference samples, we could assign each unknown by grouping its data with the full-metal set data from AHC (Supporting Information, Figure S17). Table S3 summarizes the results of the unknown assignment. AHC correctly grouped 48 out of 50 unknowns with its corresponding metal. A group of metals that were unidentified initially were the strongly quenching ones (Os(VI), Co(II) and Cu(II)), leaving unknowns 25, 40, 42 tentatively unassigned. However, simple dilution of these last three unknowns to 5  $\mu\text{M}$  allowed us to differentiate their quenched responses, assigning them correctly to their corresponding metals (Supporting Information, Figure S18). The last two unknowns (45 and 48) are assigned to Zr(IV), and no metal was assigned to In(III), leaving these last two metals undifferentiated from one another. As both of them belong to family C2 to which the sensors gave low responses, it is unsurprising that they could be confused with each other.

Our experiments demonstrate diverse ODF responses, yielding sensitivity and selectivity across 57 metal ions covering most of the periodic table. We know of no prior examples of simultaneous detection and differentiation of such a large set of metal analytes at micromolar range. One previous fluorescence sensing study used relatively large numbers of metal analytes; however, that study employed 47 commercially available dyes to detect 47 cations in aqueous/organic cosolvent at 10 mM.<sup>24</sup> In contrast, the current experiments show that only six fluorescent sensors can distinguish an even larger set of metals. Undoubtedly, the high electronic complexity of the ODF chromophores contributes to the diverse responses from each sequence. Moreover, the current chemosensors on beads were able to differentiate 50 analytes at 100-fold lower concentration than the previous study. We hypothesize that this high sensitivity is due to the monomer designs that contain relatively high-affinity fluorescent ligands.

The ODFs' multichromophore structure contributes favorably to the response diversity by yielding emission across the visible spectrum and therefore, allowing us to gather data in three broad color channels. Indeed, we observed that even a single sensor compound could discriminate as many as 15 different metal species (Supporting Information, Figure S12). It is likely that in the future, one could measure responses at finer granularity than three channels by use of more sophisticated wavelength/intensity analysis; this could allow for yet greater diversity of responses, making possible the detection of an even larger number of analytes or discriminating complex mixtures (even closely related ones) from one another. Despite the complexity of their fluorescence emission behavior, all of the current ODFs are excited at a single wavelength and analyzed using only one filter set.

The use of ODFs on solid support, as opposed to dissolved in solution,<sup>10</sup> offers the advantage of consuming extremely small amounts of material per experiment. With the current 130  $\mu\text{m}$  beads, a sensing measurement requires only  $\sim 1$  pmole of sensor and small volume of analyte (50  $\mu\text{L}$  is feasible without a specialized compartment). A single synthesis run of an ODF generates approximately  $5 \times 10^5$  beads, so cost per experiment

is very small. In addition, the use of the ODFs on solid support also enables the use of a simple microscope with RGB camera to quantify results as opposed to a spectrophotometer. One potential limitation of localizing these ODF sensors on PEG-PS beads may be the kinetics of analyte diffusion and binding. Although we observed fluorescence changes in 1 h during screening, the number of metals that our sensors responded to increased from 37 to 50 as we changed our incubation time from 1 to 24 h. It is possible that the beads, as opposed to inherently slow ligand-metal binding kinetics, contributed to this slower response. In the future it may be advantageous to test higher temperatures and mixing or flow strategies to enhance response rates.

In conclusion, we have employed a fluorescent DNA-like combinatorial library to screen for fluorescence responders to metal ions. We demonstrated the differentiating power of ODFs with simultaneous discrimination of 50 metals at 100  $\mu$ M and 30 metals at 5  $\mu$ M. In a blind test scenario, we were able to identify 48 out of 50 metals by only using 6 fluorescent probes. In the future, it will be of interest to examine the mechanisms of metal detection for ODFs, especially for those metals that show similar responses. In addition, as our study included a single ion per experiment, it will be interesting to see how a mixture of metal ions would affect the sensor responses as a relative strength of pattern-based chemosensing is the ability to respond to and differentiate complex mixtures.<sup>25</sup>

## ■ ASSOCIATED CONTENT

### ● Supporting Information

$\Delta$ RGB response data, DA plot for 100  $\mu$ M transition metals, AHC plots for cross-screening, titration curves, unknown testing and concentration curves for the selected metals. This material is available free of charge via the Internet at <http://pubs.acs.org>.

## ■ AUTHOR INFORMATION

### Corresponding Author

kool@stanford.edu

### Present Address

<sup>†</sup>Institute of Pharmaceutical Sciences, Department of Chemistry and Applied Biosciences, ETH Zurich

### Notes

The authors declare no competing financial interest.

## ■ ACKNOWLEDGMENTS

We thank Eni S.p.A. and the U.S. National Institutes of Health (R01 GM067201) for support.

## ■ REFERENCES

- (1) Aoki, S.; Kagata, D.; Shiro, M.; Takeda, K.; Kimura, E. *J. Am. Chem. Soc.* **2004**, *126*, 13377.
- (2) Gunnlaugsson, T.; Davis, A. P.; O'Brien, J. E.; Glynn, M. *Org. Lett.* **2002**, *4*, 2449.
- (3) Ma, Y.; Li, H.; Peng, S.; Wang, L. *Anal. Chem.* **2012**, *84*, 8415.
- (4) Stewart, S.; Ivy, M. A.; Anslyn, E. V. *Chem. Soc. Rev.* **2014**, *43*, 70.
- (5) Lim, S. H.; Feng, L.; Kemling, J. W.; Musto, C. J.; Suslick, K. S. *Nat. Chem.* **2009**, *1*, 562.
- (6) De, M.; Rana, S.; Akpinar, H.; Miranda, O. R.; Arvizo, R. R.; Bunz, U. H. F.; Rotello, V. M. *Nat. Chem.* **2009**, *1*, 461.
- (7) Hewage, H. S.; Anslyn, E. V. *J. Am. Chem. Soc.* **2009**, *131*, 13099.
- (8) Samain, F.; Dai, N.; Kool, E. T. *Chem.—Eur. J.* **2011**, *17*, 174.
- (9) Gao, J.; Strässler, C.; Tahmassebi, D.; Kool, E. T. *J. Am. Chem. Soc.* **2002**, *124*, 11590.

- (10) Tan, S. S.; Kim, S. J.; Kool, E. T. *J. Am. Chem. Soc.* **2011**, *133*, 2664.
- (11) Jiang, W.; Wang, S.; Yuen, L. H.; Kwon, H.; Ono, T.; Kool, E. T. *Chem. Sci.* **2013**, *4*, 3184.
- (12) Koo, C.-K.; Samain, F.; Dai, N.; Kool, E. T. *Chem. Sci.* **2011**, *2*, 1910.
- (13) Koo, C.-K.; Wang, S.; Gaur, R. L.; Samain, F.; Banaei, N.; Kool, E. T. *Chem. Commun.* **2011**, *47*, 11435.
- (14) Kwon, H.; Samain, F.; Kool, E. T. *Chem. Sci.* **2012**, *3*, 2542.
- (15) Yuen, L. H.; Franzini, R. M.; Wang, S.; Crisalli, P.; Singh, V.; Jiang, W.; Kool, E. T. *Angew. Chem., Int. Ed. Engl.* **2014**, *53*, 5361.
- (16) Zhang, L.; Zhu, L. *J. Org. Chem.* **2008**, *73*, 8321.
- (17) Minta, A.; Tsien, R. Y. *J. Biol. Chem.* **1989**, *264*, 19449.
- (18) González-Vera, J. A.; Luković, E.; Imperiali, B. *J. Org. Chem.* **2009**, *74*, 7309.
- (19) Kim, S. J.; Kool, E. T. *J. Am. Chem. Soc.* **2006**, *128*, 6164.
- (20) Traylor, T. G.; Lee, W. A.; Stynes, D. V. *J. Am. Chem. Soc.* **1984**, *106*, 755.
- (21) Nestler, H. P.; Bartlett, P. A.; Still, W. C. *J. Org. Chem.* **1994**, *59*, 4723.
- (22) Mähler, J.; Persson, I. *Inorg. Chem.* **2012**, *51*, 425.
- (23) Meuwis, K.; Boens, N.; De Schryver, F. C.; Gallay, J.; Vincent, M. *Biophys. J.* **1995**, *68*, 2469.
- (24) Lee, J. W.; Lee, J.-S.; Kang, M.; Su, A. I.; Chang, Y.-T. *Chem.—Eur. J.* **2006**, *12*, 5691.
- (25) Adams, M. M.; Joyce, L. A.; Anslyn, E. V. *Uses of Differential Sensing and Arrays in Chemical Analysis. Supramolecular Chemistry: From Molecules to Nanomaterials*; Wiley: New York, NY, 2012.